Supporting Information

Facile Fabrication of a Silver Nanoparticle-Immersed, Surface-Enhanced Raman Scattering-Imposed Paper Platform through Successive Ionic Layer Absorption and Reaction for On-Site Bioassays

Wansun Kim[a], Yeon-Hee Kim[b], Hun-Kuk Park[a,c], and Samjin Choi[a,c]*

[a]Department of Medical Engineering, Graduate School, Kyung Hee University, Seoul, 02447, Korea
[b]Department of Obstetrics & Gynecology, The Catholic University of Korea, Kyonggi-do, 11765, Korea
[c]Department of Biomedical Engineering, College of Medicine, Kyung Hee University, Seoul, 02447, Korea

***Address for correspondence:**
Samjin Choi, Ph.D.,
Department of Biomedical Engineering,
College of Medicine,
Kyung Hee University,
26, Kyungheedae-ro, Dongdaemun-gu,
Seoul, 02447, Korea
Tel: +82 2 961 0290
Fax: +82 2 6008 5535
E-mail: medchoi@khu.ac.kr

■ Potential of a SILAR-fabricated SERS Paper Platform

Table S1. SERS performance with fabrication methods based on nanoparticles*

No.	printing	NPs	process (min)	SERS EF	reproducibility (RSD, %)	ref.
1	inkjet	Ag	SCPP: 10	~10^7	-	1
2	screen	Ag	SCPP: 25	4.4×10^6	10	2
3	screen	Au	SCPP: 20	1.8×10^4	4.7	3
4	spray	Ag	SCPP: 30	2×10^7	14.5	4
5	brushing	Ag	SCPP: 60	2.2×10^7	13.4	5
6	pen	Ag	SCPP: 60	2×10^5	20	6
7	dipping	Au	SCPP: 900	5×10^6	15	7
8	dipping	Au	SCPP: 1460	2×10^8	-	8
9	dipping	Au	SCPP: 135	-	15	9
10	dipping	Au	SCPP: 15	-	8.7	10
11	**floating**	**Ag**	**SILAR: 12**	**1.1×10^9**	**4.2**	**this study**

*SCPP, synthesis-centrifugation-preparing solution-printing sequential process

■ Design Concept

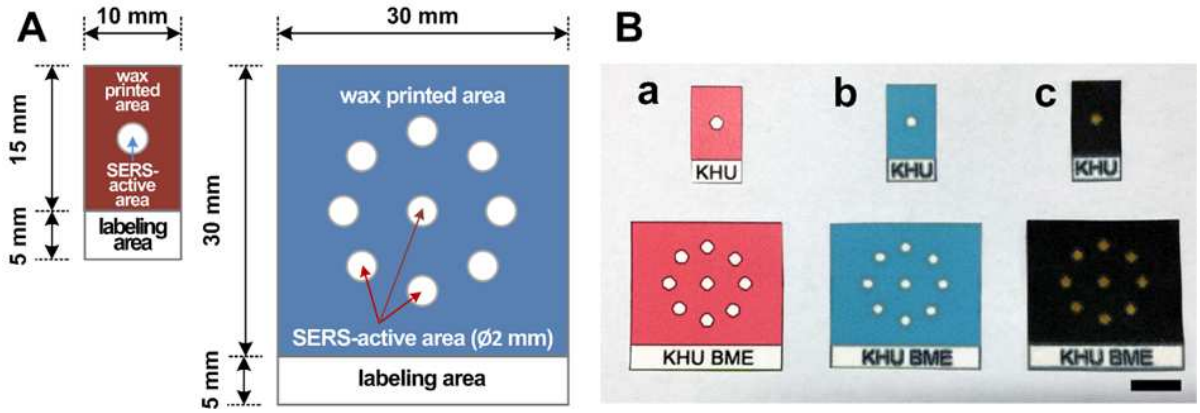

Figure S1. Scheme of the SILAR-synthesized silver nanoparticle (AgNP) SERS platform. (A) Design of the SERS paper platform. Photo (Ba) before and (Bb) after wax impregnation and (Bc) after AgNP-based SILAR printing on the paper substrate. The wax-based platform has many advantages for paper-based device fabrication and operation including non-toxicity, convenience, speed, low-cost, and visual effect. Scale bar=10 mm.

■ Substrate Selection

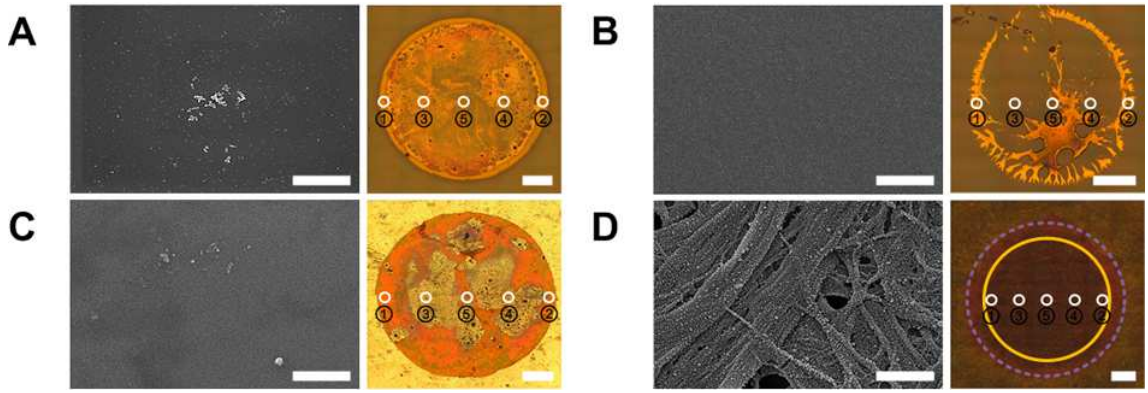

Figure S2. FE-SEM images and photographs of a dried 1-μL, 1-mM rhodamine B (RhB) droplet of AgNPs synthesized directly through the SILAR method on (A) glass, (B) PDMS, (C) Si wafer, and (D) paper substrate. (FE-SEM) Scale bar=300 μm. (Photo) Scale bar=1 μm. Yellow and purple circles on the paper substrate indicate the SERS-active and SERS-inactive areas, respectively.

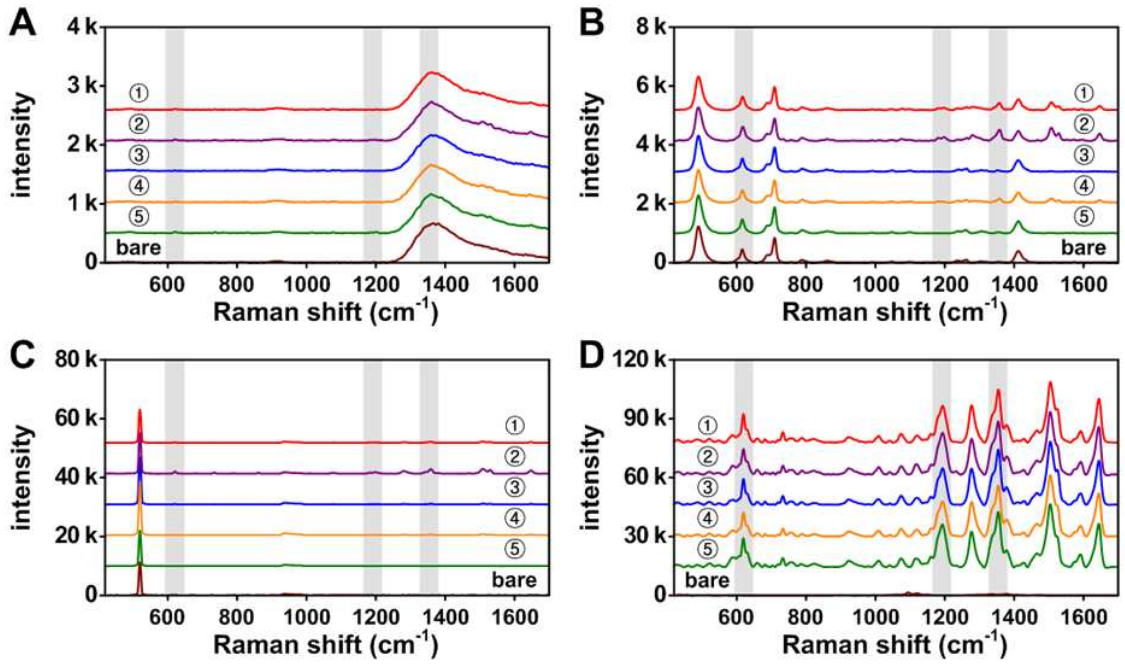

Figure S3. Position-to-position Raman spectra corresponding to Figure S2. The glass, PDMS, and Si wafer substrates demonstrated no dispersion of AgNPs, a coffee ring effect, and irregular Raman spectra, while the paper substrate produced well-dispersed AgNPs, no coffee ring effect, higher Raman intensities, and high reproducibility. Three Raman peaks indicate the characteristic peaks of RhB at 620, 1201, and 1356 cm^{-1}, associated with aromatic bending, aromatic C–H bending, and aromatic C–C stretching, respectively.

■ Optimization of the SILAR Conditions

Table S2. Optimization of two SILAR reagent concentrations, $AgNO_3$ and $NaBH_4$, at seven conditions*

SILAR solution			Raman intensity of RhB@1356 cm^{-1}		
condition	$AgNO_3$ (mM)	$NaBH_4$ (mM)	mean	SD	RSD (%)
#1	10	10	9038	2509	27.8
#2	10	20	20184	2202	10.9
#3	10	40	10990	3481	31.7
#4	**20**	**10**	**36521**	**8284**	**22.7**
#5	**20**	**20**	**29140**	**2989**	**10.3**
#6	40	10	24112	5052	21.0
#7	40	20	21446	4917	23.0

*SD, standard deviation. RSD, relative standard deviation. RhB, rhodamine B

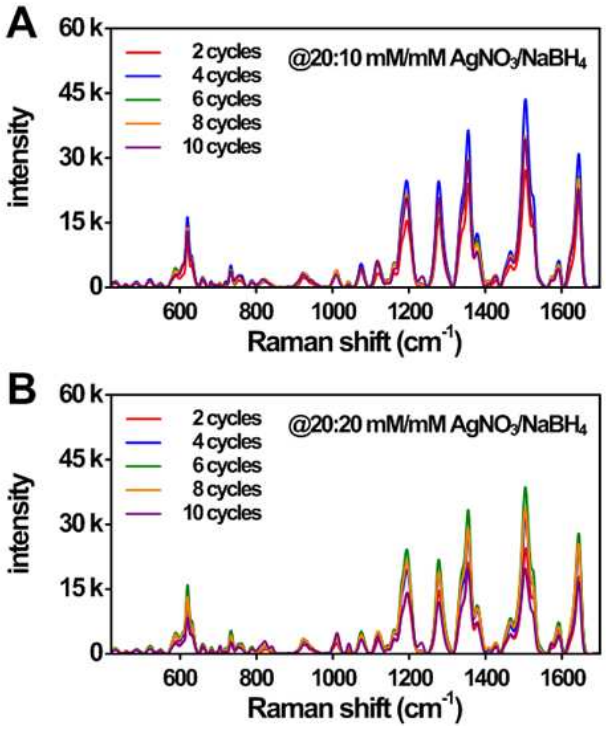

Figure S4. Raman spectra with 1-mM RhB and 2–10 SILAR cycles at (A) 20/10 and (B) 20/20 mM/mM $AgNO_3$/$NaBH_4$.

Table S3. Optimization of number of SILAR cycles at Condition #4 (20/10 mM/mM $AgNO_3/NaBH_4$) and Condition #5 (20/20 mM/mM $AgNO_3/NaBH_4$)

SILAR cycles		**Raman intensity of RhB@1356 cm^{-1}**		
condition	cycles	mean	SD	RSD (%)
	2	23971	6765	28.2
#4	4	36411	8392	23.0
$AgNO_3/NaBH_4$	6	29369	8054	27.4
(20/10 mM/mM)	8	29743	3300	11.1
	10	29330	4543	15.5
	2	21149	4739	22.4
#5	4	28243	4659	16.5
$AgNO_3/NaBH_4$	**6**	**33363**	**3696**	**11.1**
(20/20 mM/mM)	8	29140	2989	10.3
	10	19718	4796	24.3

■ Evaluation of the Optimized SILAR Conditions

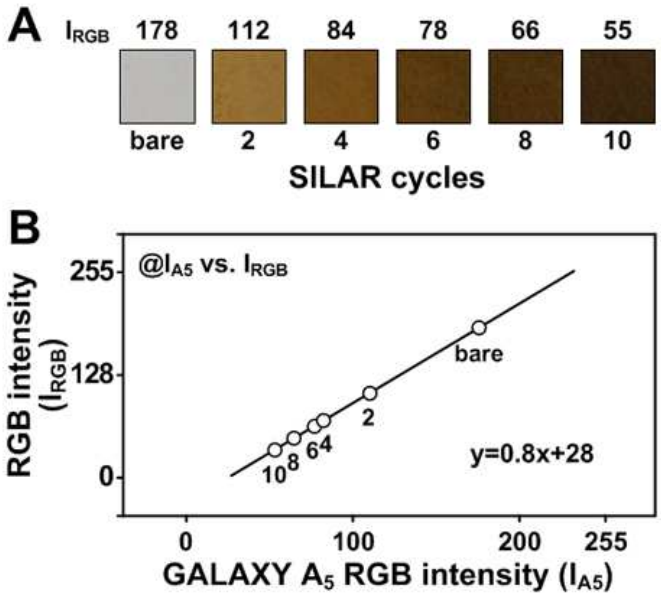

Figure S5. (A) Photographs of the paper surfaces with different numbers of SILAR cycles, and (B) compensation curve of RGB intensities. I_{A5} indicates the RGB intensity of images as acquired by a SAMSUNG GALAXY A_5 smartphone. I_{RGB} indicates the compensated RGB intensity.

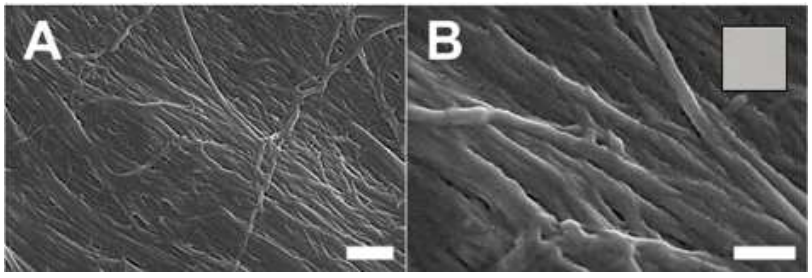

Figure S6. FE-SEM image of bare paper. (A) Scale bar=500 nm. (B) Scale bar=200 nm. Inset is a photograph of the bare paper surface.

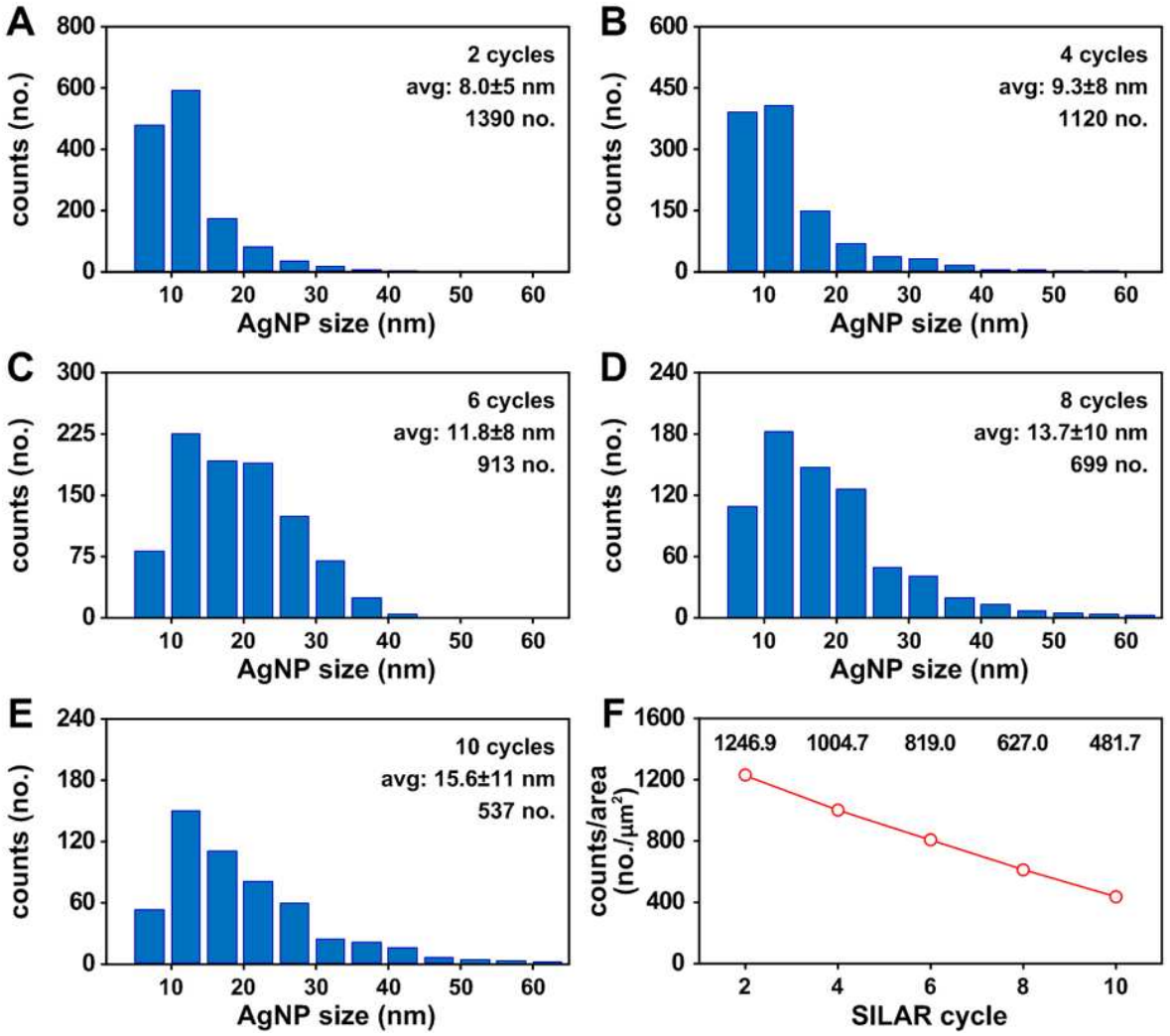

Figure S7. The size distribution and number of SILAR-synthesized AgNPs with (A) 2, (B) 4, (C) 6, (D) 8, and (E) 10 SILAR cycles. (F) The number of AgNPs per unit (no./μm^2) according to SILAR cycles.

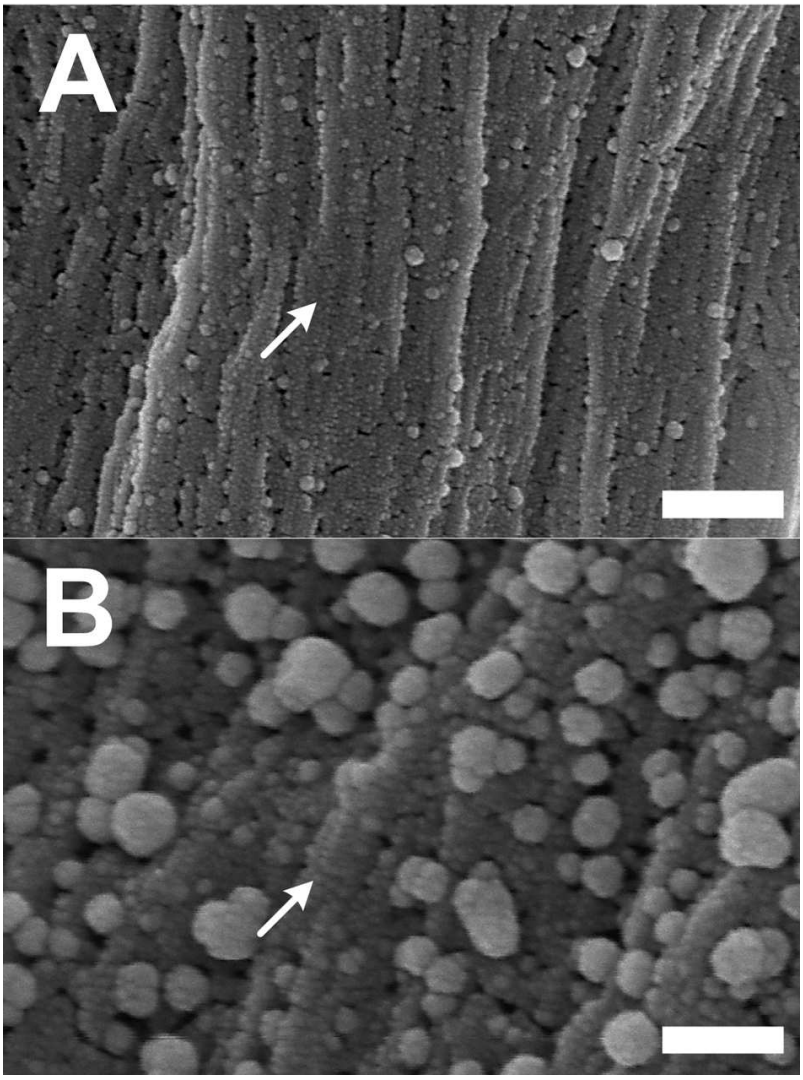

Figure S8. FE-SEM images of SILAR-synthesized tiny AgNPs with (A) 2 and (B) 6 SILAR cycles. (A) Scale bar=200 nm. (B) Scale bar=80 nm. The presence of tiny AgNPs (arrows) could be observed in both SILAR cycles.

■ Reproducibility

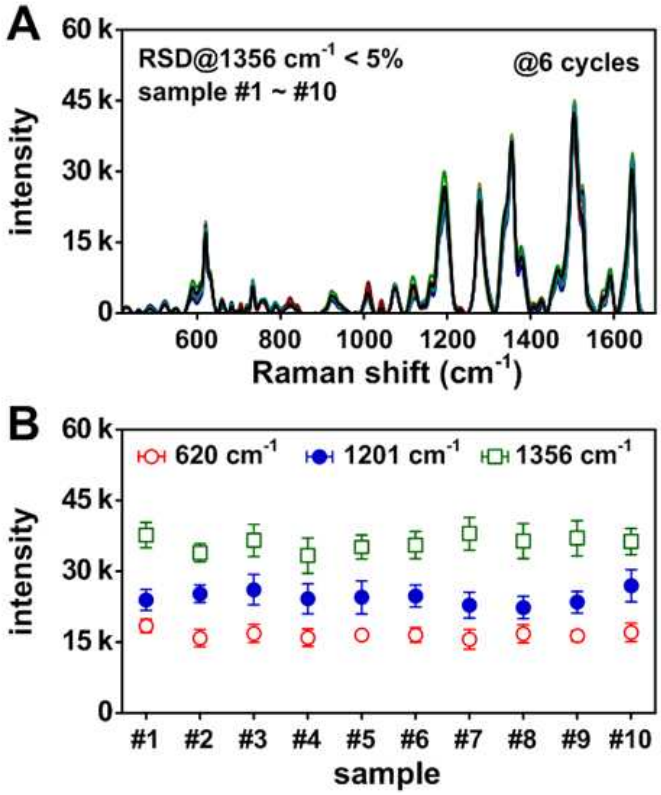

Figure S9. (A) Reproducibility and (B) three prominent RhB-characterized peaks of the SILAR-fabricated SERS paper platform at the optimized conditions (six cycles with 20/20 mM/mM $AgNO_3/NaBH_4$). The RSD of the Raman intensities of the RhB probe at 1356 cm^{-1} of 10 different SILAR samples was 4.20%.

■ Sensitivity

Table S4. Raman intensities with different concentrations of RhB probe at 1356 cm^{-1}

RhB concentration		Raman intensity of RhB@1356 cm^{-1}		
		mean	SD	RSD (%)
mM	10^{-3}	33363	3696	11.1
μM	10^{-4}	12324	1057	8.6
	10^{-5}	7584	874	11.5
	10^{-6}	3328	784	23.6
nM	10^{-7}	2029	679	33.4
	10^{-8}	1375	552	40.1
	10^{-9}	909	381	41.9
pM	10^{-10}	483	209	43.2
	10^{-11}	239	105	44.0
	10^{-12}	93	45	48.7

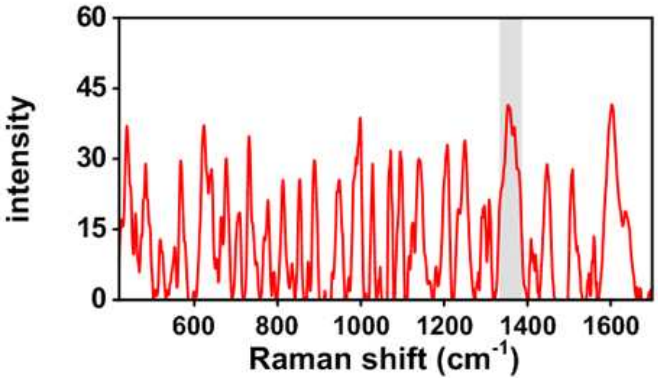

Figure 10. Raman spectra of 100 fM RhB on SILAR-synthesized AgNPs SERS paper. The presence of RhB-characterized peak at 1356 cm^{-1} at a 100-fM RhB concentration could be clearly detect due to low signal-to-noise ratio.

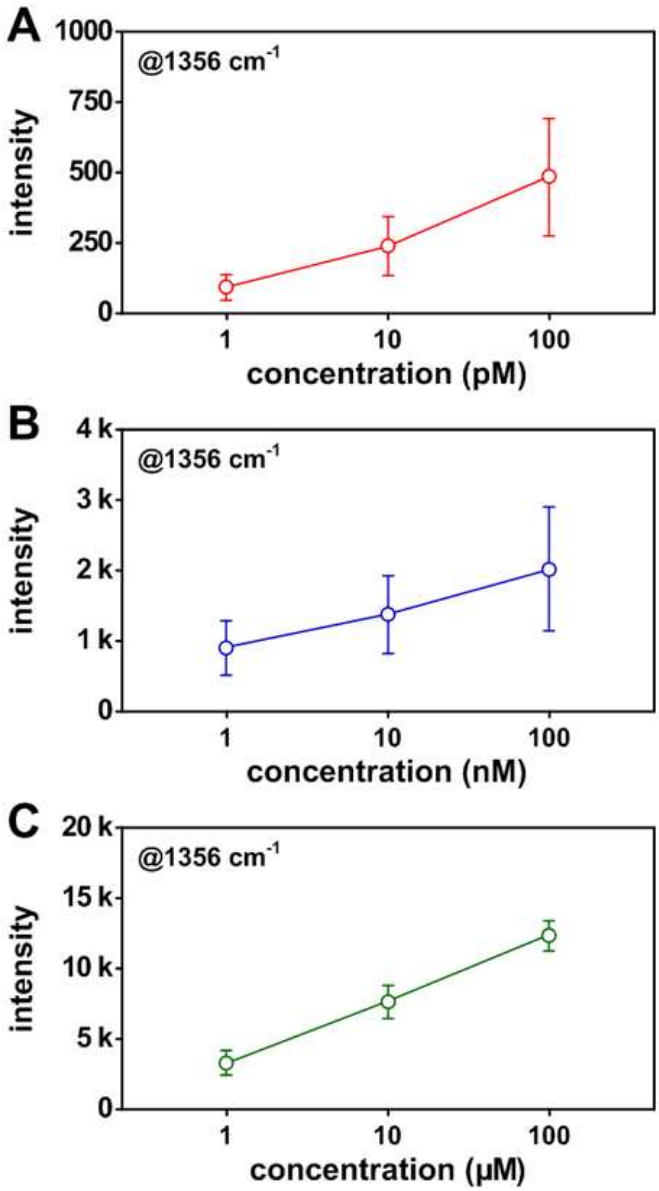

Figure S11. Raman intensities at (A) pico-scale, 1–100 pM, (B) nano-scale, 1–100 nM, and (C) micro-scale, 1–100 μM concentrations. The characteristic curves were (A) y=–749+117.8 $ln(x$+0.002) with R^2=0.99 for the pico-scale, (B) y=–11700+2086 $ln(x$+344) with R^2=0.99 for the nano-scale, and (C) y=644+299.8 $ln(x$+1.4), R^2=0.99 for the micro-scale.

■ SERS Enhancement Factor

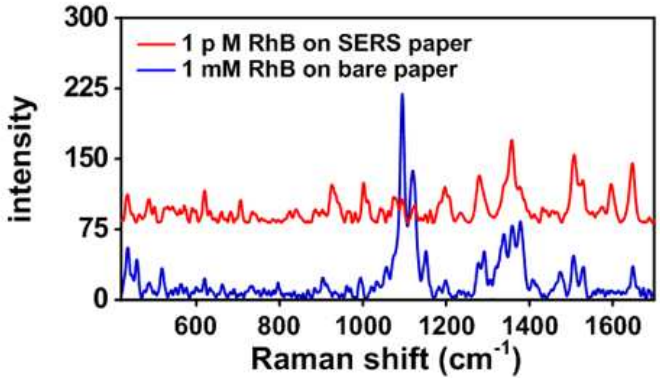

Figure 12. Raman spectra of 1-pM and 1-mM RhB on SILAR-synthesized AgNPs SERS paper and bare paper.

The enhancement factor (EF) was calculated as the difference in Raman intensity between two different substrates;

$$EF = \left(\frac{I_{SERS}}{I_{bare}} \right) \left(\frac{N_{bare}}{N_{SERS}} \right) \tag{S1}$$

where I_{SERS} and I_{bare} were the Raman intensity of the molecule on the SERS and bare papers, respectively, and N_{SERS} and N_{bare} were the average number of adsorbed molecules in the scattering volume for SERS and non-SERS areas, respectively.[11] Assuming that the probe molecules were uniformly distributed on the substrates, the number of adsorbed molecules can be estimated as

$$N = \left(N_A \cdot c \cdot \frac{V_{droplet}}{A_{spot}} \right) A_{laser} \tag{S2}$$

where N_A is Avogadro's constant, c is the concentration of the probe molecule, V is the volume of the molecule droplet, A_{spot} is the size of the substrate, and A_{laser} is the size of the laser spot.[12,13] Since the same methods for assessing the Raman measurement were applied to two substrates, the parameters of N_A of RhB, V, A_{spot}, and A_{laser} were the same. Hence, Eq. (S2) can be written as

$$EF = \left(\frac{I_{SERS}}{I_{bare}} \right) \left(\frac{c_{bare}}{c_{SERS}} \right) \tag{S3}$$

where c_{SERS} and c_R were the concentration of RhB on the SERS and bare papers, respectively.

■ On-Site Bioassays

Selection of HPV Patients

Fifteen non-pregnant female patients (age range, 22–55 years) who underwent HPV testing with the Anyplex™ II HPV28 Detection kit (Seegene, Seoul, Korea) within the previous four weeks at the Gynecology Clinic of The Catholic University of Korea, Uijeongbu St. Mary's Hospital, Uijeongbu, Korea, were enrolled in this study. Informed consent for the use of cervical specimens for research was obtained from all patients. All procedures involving humans adhered to the Declaration of Helsinki and were approved by the Ethical Committee of the Catholic Medical Center (UC14TISF0053). Patients were assigned to three experimental groups: five HPV-16 infected patients (HPV-16 group), five HPV-52 infected patients (HPV-52 group), and five HPV-58 infected patients (HPV-58 group).

Collection of Cervical Cells

Cervical cell samples were collected using a combination endocervical brush and plastic spatula device with a detachable head according to the standard collection procedure provided by the manufacturer (BD SurePath™ liquid-based Pap test; Becton-Dickinson, Franklin Lakes, NJ, USA). Two brush heads for each patient were preserved in SurePath™ Preservative Fluid (Becton-Dickinson) for further investigation. HPV infection was identified by Pap smear screening. One preserved cervical sample was mixed by vortexing to homogenize the sample and was enriched by centrifugal sedimentation with a density reagent. Non-diagnostic debris and excess inflammatory cells were partially removed from the samples. After centrifugation, the pelleted cells were resuspended, mixed, and transferred to a PrepStain™ Settling Chamber (Becton-Dickinson) mounted on a microscopic slide. The slide was cleared with xylene and covered with a cover slip. The cells were examined with a microscope by two pathologists.

Preparation of Human Cervical Fluids

The head of the brush from the other preserved cervical sample was placed inside a 15-ml conical tube. Cervical fluids were extracted from the saturated brush through centrifugation at 8,000 rpm for 15 min. The brush was carefully removed, and the cervical fluid was aspirated. Cervical samples were stored in an Eppendorf tube sealed with Parafilm® (Pechiney Plastic Packaging Company, Chicago, IL, USA) before analysis.

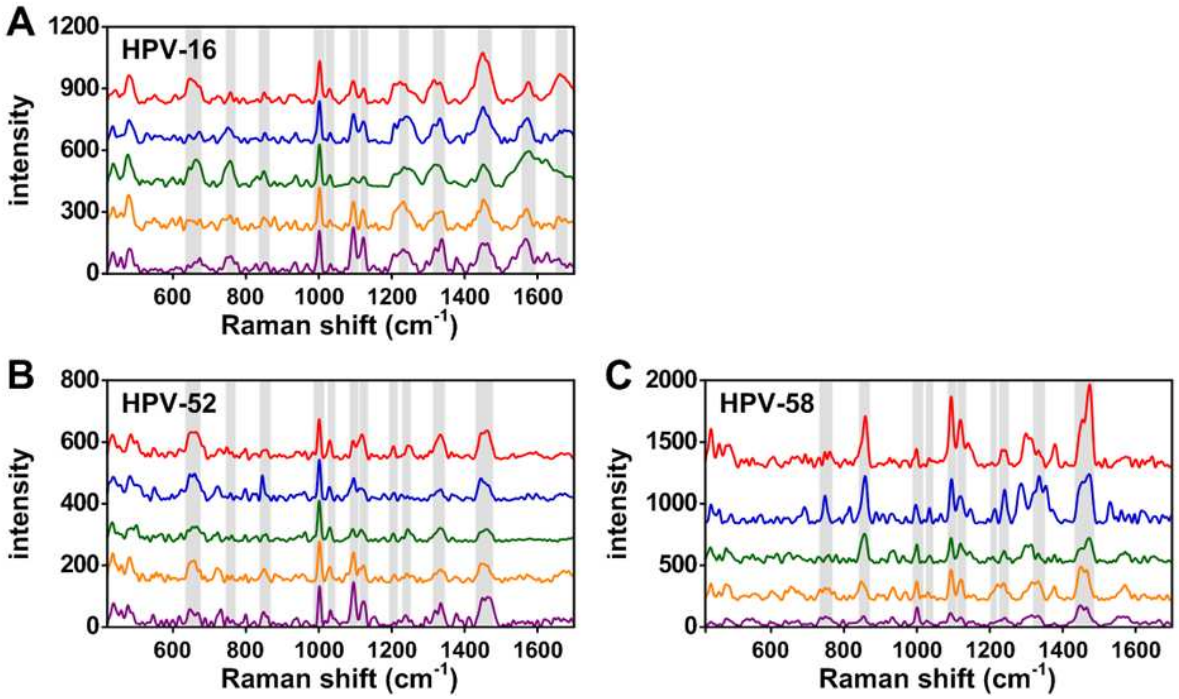

Figure S13. SERS spectra of the three most commonly observed HPV subtypes on SILAR-synthesized AgNP SERS paper: (A) HPV-16, (B) HPV-52, and (C) HPV-58.

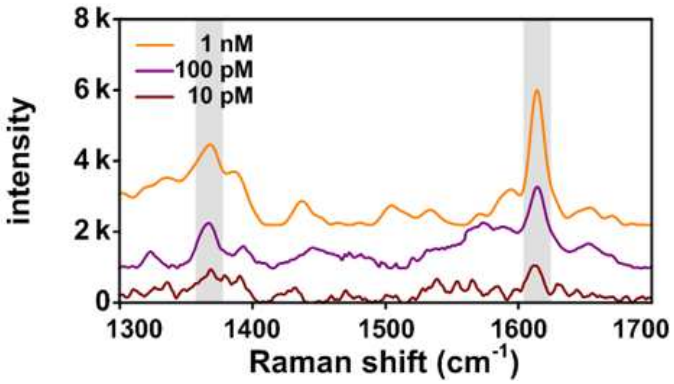

Figure S14. Representative SERS spectra with low concentrations of <1 nM MG on SILAR-synthesized AgNP SERS paper.

Table S5. Peak assignment of the SERS spectra for human papillomavirus (HPV)[14]

peak (cm^{-1})	assignment	HPV type		
		16	**52**	**58**
659	thymine ring angle bend	16	52	
750	tryptophan ring breath			58
853	tryosine ring breath	16	52	58
1003	phenylalanine symmetric ring breath	16	52	58
1094	C–N stretching in proteins, chain C–C stretching in proteins, and C–O stretching in carbohydrates	16	52	58
1120-1127	C–N and C–C stretching in proteins	16		58
1204	$C–C_6H_5$ stretching phenylalanine, tryptophan		52	
1242	amide III β-sheet	16	52	58
1342	C–H deformation in proteins	16	52	58
1448	C–H deformation in DNA/RNA, proteins, lipids and carbohydrates	16	52	58
1556	O_2 stretching	16		
1660	amide I α-helix	16		

Table S6. Peak assignment of the SERS spectra for malachite green (MG)[15]

peak (cm^{-1})	assignment
438	phenyl-C-phenyl out-of-plane bending
798	ring C–H out-of-plane bending
916	ring C–H out-of-plane bending
1172	ring C–H in-plane bending
1365	N-phenyl stretching
1613	**ring C–C stretching**

■ Life Time

Table S7. SERS activity of untreated and OTS-treated AgNP SERS papers

time (day)	untreated	degradation (%)	OTS-treated	degradation (%)
0	44763	100	48122	100
1	35478	79	44281	92
3	18303	41	29794	62
7	14684	33	23297	48
14	14231	32	21828	45
60	**13350**	**30**	**20930**	**44**

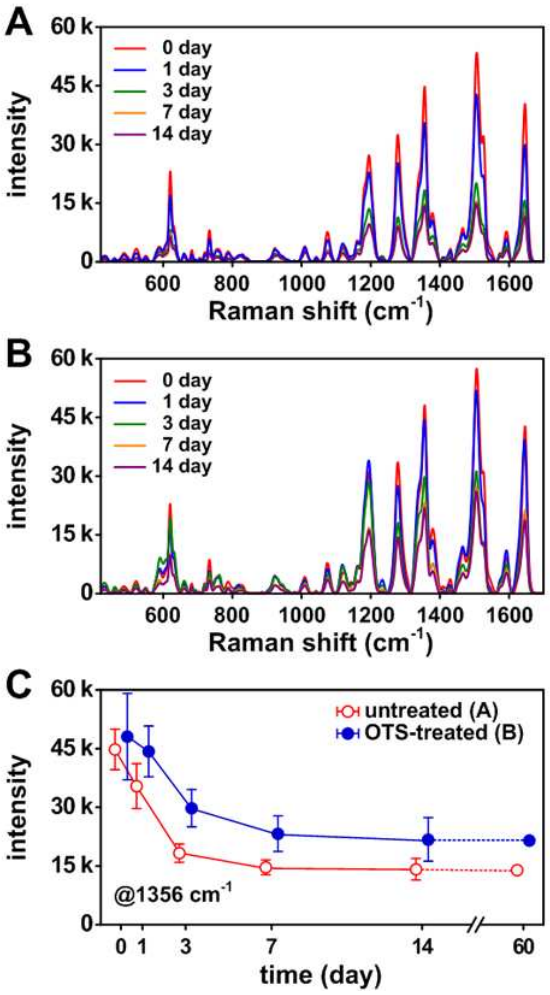

Figure S15. (C) Day-to-day variations in SERS activity between (A) untreated and (B) OTS-treated AgNP SERS papers.

■ References

(1) Yu, W. W.; White, I. M. Inkjet Printed Surface Enhanced Raman Spectroscopy Array on Cellulose Paper. *Anal. Chem.* **2010**, *82*, 9626–9630.

(2) Qu, L.-L.; Li, D.-W.; Xue, J.-Q.; Zhai, W.-L.; Fossey, J. S.; Long, Y.-T. Batch Fabrication of Disposable Screen Printed SERS Arrays. *Lab Chip* **2012**, *12*, 876–881.

(3) Kim, W.-S.; Shin, J.-H.; Park, H.-K.; Choi, S. A Low-Cost, Monometallic, Surface-Enhanced Raman Scattering-Functionalized Paper Platform for Spot-on Bioassays. *Sensors Actuators B Chem.* **2015**.

(4) Li, B.; Zhang, W.; Chen, L.; Lin, B. A Fast and Low-Cost Spray Method for Prototyping and Depositing Surface-Enhanced Raman Scattering Arrays on Microfluidic Paper Based Device. *Electrophoresis* **2013**, *34*, 2162–2168.

(5) Zhang, W.; Li, B.; Chen, L.; Wang, Y.; Gao, D.; Ma, X.; Wu, A. Brushing, a Simple Way to Fabricate SERS Active Paper Substrates. *Anal. Methods* **2014**, *6*, 2066–2071.

(6) Polavarapu, L.; Porta, A. La; Novikov, S. M.; Coronado-Puchau, M.; Liz-Marzán, L. M. Pen-on-Paper Approach toward the Design of Universal Surface Enhanced Raman Scattering Substrates. *Small* **2014**, *10*, 3065–3071.

(7) Lee, C. H.; Hankus, M. E.; Tian, L.; Pellegrino, P. M.; Singamaneni, S. Highly Sensitive Surface Enhanced Raman Scattering Substrates Based on Filter Paper Loaded with Plasmonic Nanostructures. *Anal. Chem.* **2011**, *83*, 8953–8958.

(8) Ngo, Y. H.; Li, D.; Simon, G. P.; Garnier, G. Gold Nanoparticle-Paper as a Three-Dimensional Surface Enhanced Raman Scattering Substrate. *Langmuir* **2012**, *28*, 8782–8790.

(9) Zheng, G.; Polavarapu, L.; Liz-Marzán, L. M.; Pastoriza-Santos, I.; Pérez-Juste, J. Gold Nanoparticle-Loaded Filter Paper: A Recyclable Dip-Catalyst for Real-Time Reaction Monitoring by Surface Enhanced Raman Scattering. *Chem. Commun.* **2015**, *51*, 4572–4575.

(10) Zhang, K.; Zhao, J.; Xu, H.; Li, Y.; Ji, J.; Liu, B. Multifunctional Paper Strip Based on Self-Assembled Interfacial Plasmonic Nanoparticle Arrays for Sensitive SERS Detection. *ACS Appl. Mater. Interfaces* **2015**, *7*, 16767–16774.

(11) Le Ru, E. C.; Blackie, E. J.; Meyer, M.; Etchegoin, P. G. Surface Enhanced Raman Scattering Enhancement Factors: A Comprehensive Study. *J. Phys. Chem. C* **2007**, *111*, 13794–13803.

(12) Zhang, L.; Lang, X.; Hirata, A.; Chen, M. Wrinkled Nanoporous Gold Films with Ultrahigh Surface-Enhanced Raman Scattering Enhancement. *ACS Nano* **2011**, *5*, 4407–4413.

(13) Liu, X.; Shao, Y.; Tang, Y.; Yao, K.-F. Highly Uniform and Reproducible Surface Enhanced Raman Scattering on Air-Stable Metallic Glassy Nanowire Array. *Sci. Rep.* **2014**, *4*, 5835.

(14) Choi, S.; Park, H.-K.; Min, G. E.; Kim, Y.-H. Biochemical Investigations of Human Papillomavirus-Infected Cervical Fluids. *Microsc. Res. Tech.* **2015**, *78*, 200–206.

(15) Zhang, Y.; Yu, W.; Pei, L.; Lai, K.; Rasco, B. a.; Huang, Y. Rapid Analysis of Malachite Green and Leucomalachite Green in Fish Muscles with Surface-Enhanced Resonance Raman Scattering. *Food Chem.* **2015**, *169*, 80–84.